Letter

Controlling the properties of $PbTiO_3/SrTiO_3$ superlattices by photoexcited carriers

Carmel Dansou,[1] Charles Paillard,[2] and Laurent Bellaiche[1]
[1]*University of Arkansas, Fayetteville, Arkansas 72701, USA*
[2]*Université Paris-Saclay, CentraleSupélec, CNRS, Laboratoire SPMS, 91190 Gif-sur-Yvette, France*

(Received 11 June 2022; revised 15 November 2022; accepted 28 November 2022; published 12 December 2022)

The effect of light on the properties of $PbTiO_3/SrTiO_3$ superlattices is studied using first-principles calculations in their paraelectric phase *p* as well as in the, *c*, *r*, and *aa* phases that are defined by polarization lying along the [001], [11*v*], and [110] directions, respectively. While the *r* phase is the ground state in dark conditions, illumination triggers a rotation of the polarization towards the out-of-plane direction, which results in the *r* phase transforming into a *c* phase at a large concentration of photoexcited carriers. We further reveal that a space charge region of free carriers builds up at the interface under illumination, implying that these superlattices can be thought as acting as *p-i-n* junctions under light. These free charges screen the polarization discontinuity at the interface, effectively reducing the electrostatic depolarizing field.

DOI: 10.1103/PhysRevB.106.L220101

I. INTRODUCTION

$(PbTiO_3/SrTiO_3)_m$ superlattices [$(PTO/STO)_m$SLs] have gained a lot of attention [1–11]. It was found that, by tuning the epitaxial strain and the PTO volume fraction, a large variety of fascinating properties can be engineered in these SLs [1,2,4]. They have, e.g., been found to host nontrivial topological structures [7–10] and negative capacitance [12], which are of fundamental as well as practical interest [13].

There have also been significant developments in the interaction of light with ferroelectric (FE) materials during the last decade [14,15], with light having the capability to induce a structural change (photostriction) and even a phase transition in classical FE materials [14,16–19]. More recently it was also reported that one can control the topology of phonons in FE materials with light [20].

It is now natural and timely to ask whether light can modulate the physical properties of FE SLs. For example, it was reported that under illumination, PTO/STO SLs transform from a polydomain structure to a uniform domain configuration [21]. This transition was accompanied by the expansion of the out-of-plane lattice of the SLs. A light-induced polarization rotation was also evidenced at the nanoscale in multidomains [22], as well as an optically induced phase transition from a vortex and domain state to a so-called supercrystal phase in PTO/STO SLs [23]. However, light interactions with FE SLs have been mostly experimentally studied so far. To the best of our knowledge, theoretical investigations were limited to phenomenologically varying the dielectric constant of the dielectric layer to reproduce the supercrystal phase [23]. Microscopic insights are thus lacking. Many questions remain unresolved, such as what are the microscopic mechanisms favoring photoinduced transitions in these SLs or changes in their physical properties under light.

Here, we explore light interactions with monodomain $(PbTiO_3/SrTiO_3)_m$ SLs. Technically, we apply our recently developed scheme to mimic the effect of photoinduced thermalized carriers [24] on the relative energy and phase stability of different phases having different electrical polarization orientations. We observe photoinduced phase transitions and changes in properties, and further reveal their microscopic origins via the development of an analytical model demonstrating that these SLs can be thought as *p-i-n* junctions when under illumination.

II. METHODS

A. Constrained density functional theory

The constrained density functional theory (c-DFT) is a purpose built method to simulate photoexcitation in pump-probe optical experiments within the known DFT framework. Photoexcited thermalized electrons and holes are described using the Fermi-Dirac distribution with two chemical potentials, μ_e for electrons and μ_h for holes. During the self-consistent field (SCF) DFT cycles, the electronic density is converged with the constraint of having $n_e = n_{\rm ph}$ electrons per formula unit in the conduction band and $n_h = n_{\rm ph}$ holes in the valence band. Explicitly one solves numerically for the couple of chemical potentials (μ_e, μ_h) using the following equations at each SCF cycle:

$$n_h = \sum_{i \leqslant N_v} \sum_{k,\sigma} w_k [1 - f(\epsilon_{ik,\sigma}, \mu_h)], \tag{1}$$

$$n_e = \sum_{i > N_v} \sum_{k,\sigma} w_k f(\epsilon_{ik,\sigma}, \mu_e). \tag{2}$$

w_k is the weight of the k point $\mathbf{k}$, $f(\epsilon_{ik,\sigma})$ is the occupation number, σ stands for spin, and N_v is the index of the highest occupied band [24]. This scheme, recently implemented in the ABINIT package, has proven to successfully mimic the effects of photoexcited carriers in ferroelectrics [24].

B. Computational details

We performed DFT calculations as implemented in the ABINIT package [25] with the projector augmented-wave

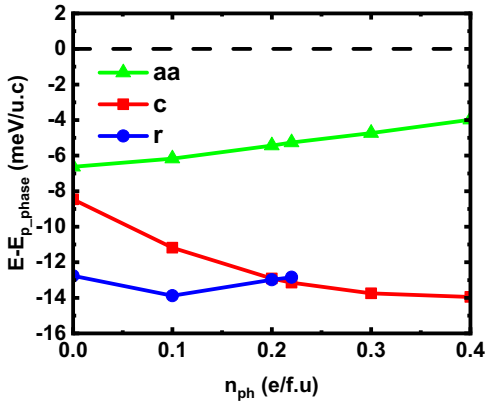

FIG. 1. Relative energies of the different phases. The zero of energy is chosen to be that of the p phase, for any illumination.

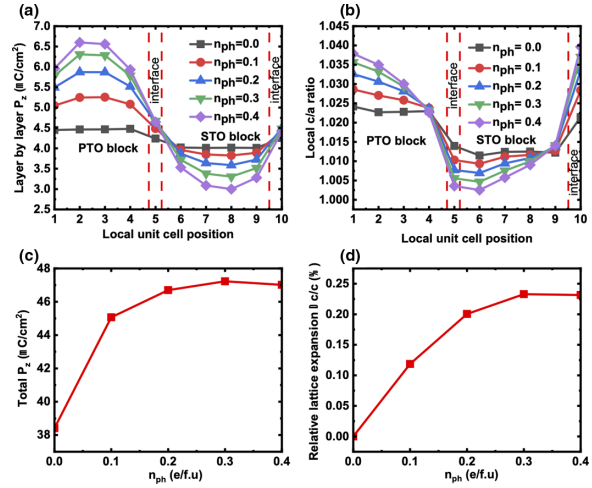

FIG. 2. (a) Layer-by-layer polarization, (b) local out-of-plane lattice distortion, (c) total polarization, and relative lattice expansion in the c phase.

method [26]. The generalized gradient approximation with the Perdew-Burke-Ernzerhof parametrization revised for solids was used as the exchange-correlation functional [27]. A 20 hartree plane-wave cutoff was employed in our calculations. A $6\times6\times1$ k mesh equivalent to a $6\times6\times6$ mesh in a five-atom unit cell allows us to reach convergency for both forces and energies. Density was considered converged when the difference of forces on atoms between two self-consistent field iterations is less that 1×10^{-7} hartree bohr^{-1}. Both cell shapes and ionic positions were further optimized until the maximum forces on the ions were less than 2×10^{-5} hartree bohr^{-1}.

We simulated monodomains in $(PTO)_5/(STO)_5$ SLs that are built by stacking along the [001] direction five unit cells of PTO and five unit cells of STO. The choice of 5/5 PTO/STO SLs as a model for this study is inspired by previous studies and our computational resources. When simulating a light interaction with the superlattices, calculations become very heavy for larger supercells. As such we had to choose the size of the superlattices to be thick enough but in accordance with the resource's constraints. Also, a 5/5 PTO/STO film has been experimentally grown [11], which demonstrates the experimental relevance of our choice. The in-plane lattice constant was kept fixed at the theoretical optimized lattice constant of STO, in order to mimic a growth on a STO substrate. First, the SLs were optimized to find a reference paraelectric structure with mirror symmetry called the p phase [28]. Three other phases are then considered: the c phase with a polarization along the out-of-plane [001] direction, the aa phase with a polarization lying along the in-plane [110] direction, and the r phase with a polarization being along the $[uuv]$ directions [28]. Starting from the optimized structure under dark conditions, a light interaction with these phases was then simulated using the c-DFT. When under light, both the cell shape and ion positions of the structures were again relaxed with the aforementioned parameters.

III. RESULTS

A. Energy and stability

In Fig. 1, we show the relative energies of the different phases (with respect to the p reference phase) for various excited charge carriers concentration (n_{ph}). In the dark condition [$n_{ph} = 0$ electrons per formula unit (e/f.u.)], the most stable phase is the r phase where the polarization points along a specific $[11v]$ direction, such that it makes an angle $\theta \approx 72^\circ$ with the z axis. As we increase the light intensity (n_{ph}), the relative energy of the c phase gets closer to that of the r phase until the two basically coincide for n_{ph} larger than 0.2 e/f.u. As we will see later, such behaviors originate from the facts that, under light, the r phase first rotates its polarization towards the [001] direction and then transforms into the c phase that becomes the ground state. Meanwhile, the energy of the aa phase increases away from its ground state's energy, as n_{ph} increases.

B. Light-induced polarization and lattice dynamism in the c phase

To further determine the effects of light on the different phases, we also compute the polarization in a layer-by-layer fashion using the Born effective charges of the atoms in each local unit cell via

$$P_i = \frac{e}{\Omega_i} \sum_{j\in i} w_j \delta_j Z_j^*, \tag{3}$$

where Ω_i, e, and δ_j are the volume of the unit cell i, the elementary charge, and the atomic displacement from the reference paraelectric p phase, respectively. Z_j^* is the Born effective charge of the atom j, with j running through all the atoms in the cell i and w_j being a weight corresponding to the number of five-atom unit cells that share the atom j. The Born charges Z_j^* are taken from Ref. [29].

The data are shown in Fig. 2(a) for the c phase. In the dark condition, the electrical polarization throughout the SLs is nearly constant, as consistent with previous reports [30,31] and which arises from the minimization of the electrostatic cost associated with bound charges at the interfaces. Under illumination, the electrical polarization in PTO layers increases while the polarization in STO layers decreases. The polarization in the interfacial regions [unit cells 5 and 10 in

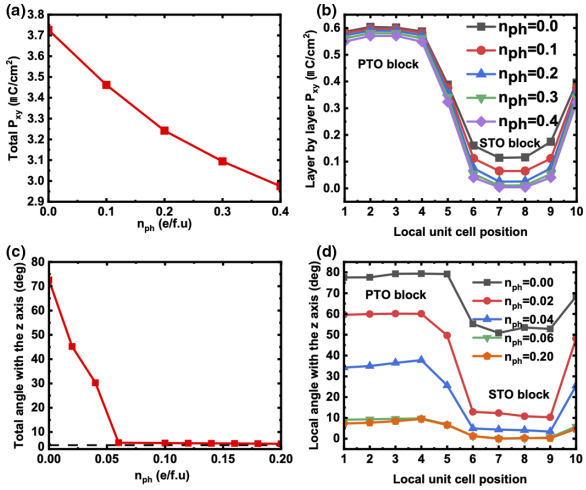

FIG. 3. (a) Total in-plane polarization and (b) local polarization, in the *aa* phase. The angle of the electrical polarization with the z axis in the r phase: (a) global angle, and (b) local angle.

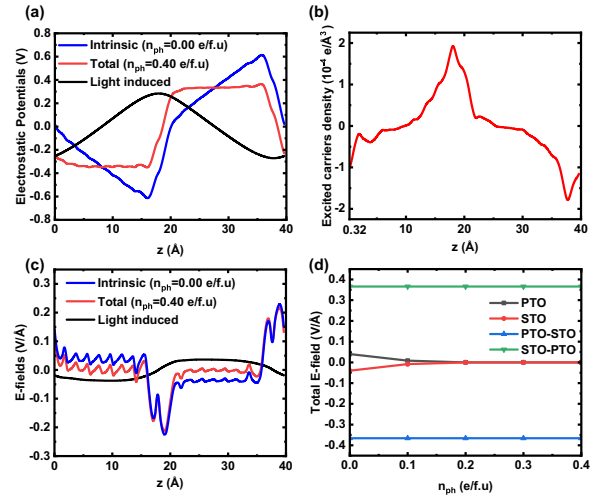

FIG. 4. (a) The different potentials for $n_{\mathrm{ph}} = 0.4\ e$/f.u. and $n_{\mathrm{ph}} = 0\ e$/f.u.; (b) the difference in the macroscopic average excited charge carrier densities between the cases of $n_{\mathrm{ph}} = 0.4\ e$/f.u. and $n_{\mathrm{ph}} = 0\ e$/f.u.; (c) E fields for $n_{\mathrm{ph}} = 0.4\ e$/f.u. and $n_{\mathrm{ph}} = 0\ e$/f.u.; (d) total E field in different parts of the SLs as a function of light intensity.

Fig. 2(a)] remains mainly unaffected. The overall polarization, however, increases with light intensity, as shown in Fig. 2(c). The increase of the polarization in the SLs is accompanied by an increase in the local out-of-plane lattice distortion in PTO layers as well as in the global out-of-plane lattice of the SLs, as revealed by Figs. 2(b) and 2(d) and as also found in an optical excitation experiment on PTO/STO SLs having multidomains [21]. The local out-of-plane distortion is quantified as $(z^i_{A_2} - z^i_{A_1})/a$ where $z^i_{A_1}, z^i_{A_2}$ are the z positions of the $A_{j=1,2}$ = Pb or Sr atoms at the corners of the cell i in the SLs with $z^i_{A_1} < z^i_{A_2}$, and a is the in-plane lattice constant of the SLs.

C. Light-induced polarization dynamism in the *aa* phase

We also looked at the *aa* phase and the effect of light on its polarization. In Figs. 3(a) and 3(b), we show the total and local in-plane polarizations of this *aa* phase, as a function of light intensity. The total electrical polarization of the *aa* phase decreases with n_{ph}, indicating that light penalizes in-plane polar displacements. This finding is also consistent with the steady increase in the energy of this *aa* phase seen in Fig. 1. Furthermore, inspection of the layer-by-layer polarization in the *aa* phase, as shown in Fig. 3(b), indicates that the decrease of its polarization mostly comes from the STO layers that tend to become paraelectric under light (in a dark condition, the STO layers are ferroelectric as a consequence of their proximity with PTO layers within our considered supercell).

D. Light-induced polarization rotation in the *r* phase

The observations from the *c* and *aa* phases imply that in the r phase, the in-plane component of the electrical polarization should be reduced while its out-of plane component should be increased by illumination. This should thus lead to the polarization in the r phase rotating towards the out-of-plane direction upon illumination, and to the transition from the r to the c phase observed in the energy diagram in Fig. 1. We map out the angle between the z axis and the electrical polarization within the r phase as a function of n_{ph}. The results shown in Figs. 3(c) and 3(d) are well consistent with our above explanations. We therefore have a light-induced polarization rotation within the r phase. A similar light-induced polarization rotation has been seen at domain boundaries in multidomain PTO/STO SLs where the polarization rotates from an r-like orientation to a c-like orientation upon optical excitation [22], in line with our predictions. In Fig. 3(d), we show the variation of the angle of the polarization with the z axis across the SLs. Under illumination, the polarization in the STO layer rotates faster towards the z axis and this angle is almost zero for all values of $n_{\mathrm{ph}} > 0.06\ e$/f.u. which indicates that, beyond a certain light intensity, the polarization in the STO layer stays practically along the z axis. Any further rotation of the polarization in the SLs beyond $n_{\mathrm{ph}} > 0.06\ e$/f.u. therefore emanates mostly from the rotation of the local polarization in the PTO layers.

E. Light-induced depolarization field screening

Next, we look at the macroaveraged [32,33] (also detailed in the Supplemental Material [34], Sec. 1) electrostatic potential and charge densities inside the c phase as a function of n_{ph}. From the macroaveraged potential, we deduce the macroaveraged internal electric field by a numerical finite-difference differentiation of the potential data with respect to z [35]. In the dark condition and as shown in Fig. 4(a) via the blue curve, there is a finite electric field in both PTO and STO layers, consistent with previous reports on FE-dielectric SLs [30,36], with short-circuit boundary conditions requiring the fields in the PTO and STO layers to be opposite in sign. It is the polarization mismatch between PTO and STO layers that induces this electric field in the STO layer [37,38]. These internal fields act as depolarizing fields limiting the polarization in the SLs. As we photoexcite charge carriers, they mainly populate the interface regions of the PTO/STO SLs as evidenced by the difference, shown in Fig. 4(b), in the macroscopic average in the charge carrier densities between

one illumination ($n_{\rm ph} = 0.4\ e$/f.u.) and dark conditions (the same trend is obtained for other values of $n_{\rm ph}$). Interfaces are populated by opposite but equal amounts of excited charge carriers. Our results agree with some existing experimental reports indicating that excited charge carriers migrate to the interfaces to screen the depolarizing field [21,22]. However, for the considered SLs thicknesses, the excited charge carriers are rather significantly localized at the interfaces while they tail into PTO and STO layers. This feature has been observed in previous studies on electron gas at $LaAlO_3/SrTiO_3$ where for a thin film, the free gas was observed to also tail into the STO layers [39,40]. Consequently, the internal electric fields in PTO and STO layers reduce their value under illumination [see the red curve versus the blue curve in Fig. 4(c)] and even quench for $n_{\rm ph}$ equal to or larger than 0.2 e/f.u., as revealed by Fig. 4(d). For each considered finite $n_{\rm ph}$, one can also define a light-induced potential that consists of the difference between the total electrostatic potential for such finite $n_{\rm ph}$ and the one for $n_{\rm ph} = 0$, as shown via the black solid lines in Fig. 4(a). Such a light-induced potential can be understood as a light-induced electric field [see Fig. 4(c) for the case of $n_{\rm ph} = 0.4\ e$/f.u.). In both PTO and STO layers, light produces fields opposite to the intrinsic internal field leading to a net zero field in these layers [Fig. 4(c)]. We therefore have a light-induced depolarizing field screening. In contrast, light has a very negligible effect on the fields at the two interfaces, as demonstrated in both Figs. 4(c) and 4(d).

F. Electrostatic model of light-induced dynamism

In the following, we propose a simple electrostatic model to account for the light-induced change in electrostatics in the SLs. For simplicity, we assume that the excited charge carriers are significantly localized and homogeneously populate the interface regions, and that PTO and STO are mainly recombination regions where there are no net excited charge carriers. In one unit cell of the SLs, the volume charge density of excited carriers can be defined as follows,

$$\rho^l(z) = \begin{cases} 0, & z_0 \leqslant z \leqslant z_1, \\ +\rho_v, & z_1 \leqslant z \leqslant z_2, \\ 0, & z_2 \leqslant z \leqslant z_3, \\ -\rho_v, & z_3 \leqslant z \leqslant z_4, \end{cases} \quad \rho_v = \frac{\int_{z_1}^{z_2} \rho(z) dz}{z_2 - z_1}. \tag{4}$$

where $\rho(z)$ are the differences in the macroaveraged charge density [see, e.g., Fig. 4(b) for the case of ($n_{\rm ph} = 0.4\ e$/f.u.)], z_0 and z_1 are the boundaries of the PTO layer, z_1 and z_2 are the boundaries of PTO-STO interface, z_2 and z_3 are the boundaries of the STO layer, and z_3 and z_4 those of the STO-PTO interface. The values of z_1, z_2, z_3, z_4 are extracted from our computational data and are $(z_0, z_1, z_2, z_3, z_4) \approx (0.32, 16.10, 20.06, 35.84, 39.63)$ Å. The above-defined charge density is similar to charge densities in a typical *p-i-n* junction in semiconductors [41–43]. Using basic electrostatic equations,

$$\frac{dE^l(z)}{dz} = -\frac{d^2V^l(z)}{dz^2} = \frac{\rho_v}{\epsilon}, \tag{5}$$

where ϵ is the static permittivity whose value changes throughout the SLs, i.e., $\epsilon = \epsilon_{\rm PTO}$ in the PTO layer, $\epsilon = \epsilon_{\rm STO}$ in the STO layer, and the average of the dielectric permittivities of PTO and STO is taken as an approximation of ϵ at the interfaces. Note, however, that we did not use any previously computed values of ϵ but rather extracted the ratio $\rho_v/\epsilon \approx 0.02$ V Å^{-2} from the slope of the computed light-induced field in the interface regions [Fig. 4(c)]. The light-induced electrostatic field and potential are as follows,

$$E^l(z) = \begin{cases} -E_0^l, & z_0 \leqslant z \leqslant z_1, \\ -E_0^l + \dfrac{z - z_1}{\epsilon}\rho_v, & z_1 \leqslant z \leqslant z_2, \\ +E_0^l, & z_2 \leqslant z \leqslant z_3, \\ E_0^l - \dfrac{z - z_3}{\epsilon}\rho_v, & z_3 \leqslant z \leqslant z_4, \end{cases}$$

$$V^l(z) = \begin{cases} (z - z_0)E_0^l + V_0, & z_0 \leqslant z \leqslant z_1, \\ V_1^l + (z - z_1)E_0^l - \dfrac{(z - z_1)^2}{2\epsilon}\rho_v, & z_1 \leqslant z \leqslant z_2, \\ V_2^l - (z - z_2)E_0^l, & z_2 \leqslant z \leqslant z_3, \\ V_3^l + (z_3 - z)E_0^l + \dfrac{(z - z_3)^2}{2\epsilon}\rho_v, & z_3 \leqslant z \leqslant z_4, \end{cases} \tag{6}$$

with $E_0^l \approx 0.036$ V Å^{-1} being the strength of the light-induced field at $z_0 = 0.32$ Å and $(V_0^l, V_1^l, V_2^l, V_3^l) \approx (-0.26, 0.26, 0.26, -0.26)$ V being the electrostatic potentials induced by light at z_0, z_1, z_2, z_3, respectively, as extracted from DFT data plotted in Figs. 4(a) and 4(b). In Fig. 5, we show the results of our analytical model and compared them with the data from our DFT computations for the highest studied light intensity ($n_{\rm ph} = 0.4\ e$/f.u.). The agreement is rather good for both the light-induced field and electrostatic potential. One can then conclude that, at the microscopic level, illuminated PTO/STO SLs act as *p-i-n* junctions with (1) the PTO-STO interface being the *p* region, (2) the STO-PTO interface being the *n* region, and (3) PTO and STO layers being the *i* regions (intrinsic zone of neutral charges sandwiched between the *p* and *n* regions). The photoinduced electric fields produced by this (*p-i-n*)-like junction in PTO and STO layers screen out the depolarization field inside the PTO and STO layers. The Supplemental

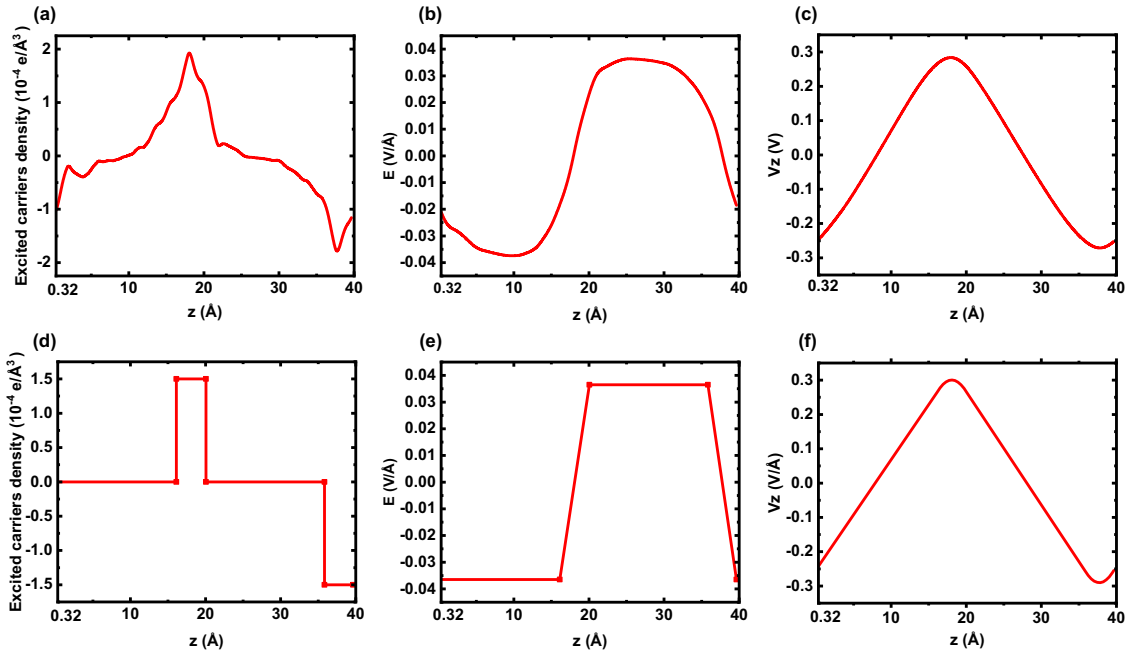

FIG. 5. Comparison between the DFT data (first row) and the presently developed analytical model (second row) about light-induced electrostatics for the case of $n_{\mathrm{ph}} = 0.4\ e/\mathrm{f.u.}$ (a) and (d) correspond to the difference in the macroaveraged charge density, (b) and (e) represent the light-induced electric field, and (c) and (f) correspond to the light-induced electrostatic potential.

Material reports the results of another model that is similar in spirit with the one described by Eq. (4) (that is, excited charge carriers are strongly localized at the interfaces) but with different forms for $\rho(z)$ (see Supplemental Material [34], Sec. 2).

IV. DISCUSSION

Here, we would like to point to some existing models proposed in the literature to produce a screening layer at the PTO/STO interface by tuning the PTO film's thickness [44–46]. In those models, the free carriers can only be produced when the electrical polarization is normal to the interface. As such, one cannot use these models to study the impact of free carriers on the electrical polarization in the *aa* and the *r* phases considered in our study.

Also, in this Letter, we did not consider oxygen octahedral rotation or tilting that are known to compete with polarization in some systems. This is mostly because we first wanted to know the effect of light on polarization alone in the studied superlattices but also because neither PTO nor STO possesses such a rotation or tilting at room temperature (which is the temperature at which the measurements are typically done). The effect of excited charge carriers on these antiferrodistortive modes and their coupling with polarization in these SLs, as well as the additional effect of varying the epitaxial strain, are interesting questions to explore for future studies.

Finally, note that in the present Letter, we limit ourselves to monodomains in these SLs in order to first reveal and understand the impact of photoexcitation on different polar phases before tackling the more complex impact of light on polydomains. The extension of this study to polydomain SLs is left for future exploration.

V. CONCLUSION

In summary, we report a first-principles investigation of the impact of light on the energetic and physical properties of monodomain $(\mathrm{PTO})_5/(\mathrm{STO})_5$ SLs. From energetics and electrostatic analysis, we now understand that the polarization in close to open-circuit conditions will grow under illumination as photoexcited carriers will screen the polarization bound charges. On the other hand, the polarization in directions close to short-circuit conditions reduces under illumination, as is reminiscent of results in bulk ferroelectrics [16]. In our specific case, this results in the polarization rotation of the *r* phase of monodomain PTO/STO SLs towards that of the *c* phase under illumination. The favoring of an out-of-plane polarization under illumination thus helps explain the transition to a monodomain state observed in Ref. [21] or the domain boundary rotation discussed in Ref. [22]. We therefore hope that the present Letter deepens the active field of light-matter interactions and can be used to design novel efficient devices using light as a physical handle since, e.g., the rotation of polarization is known to dramatically enhance many physical properties, including piezoelectricity, dielectric responses, as well as elasto-optical and electro-optical conversions [47–50].

ACKNOWLEDGMENTS

The work is supported by the ARO Grants No. W911NF-21-2-0162 (ETHOS) and No. W911NF-21-1-0113, and the Vannevar Bush Faculty Fellowship (VBFF) Grant No. N00014-20-1-2834 from the Department of Defense. C.P. is

thankful for support from a public grant overseen by the French National Research Agency (ANR) as part of the "Investissements d'Avenir" program (Labex NanoSaclay, reference: ANR-10-LABX-0035). C.P. acknowledges support from ANR grant SUPERSPIN under contract ANR-21-CE24-0032.

[1] M. Dawber, C. Lichtensteiger, M. Cantoni, M. Veithen, P. Ghosez, K. Johnston, K. M. Rabe, and J. M. Triscone, Unusual Behavior of the Ferroelectric Polarization in $PbTiO_3/SrTiO_3$ Superlattices, Phys. Rev. Lett. **95**, 177601 (2005).

[2] M. Dawber, N. Stucki, C. Lichtensteiger, S. Gariglio, P. Ghosez, and J. M. Triscone, Tailoring the properties of artificially layered ferroelectric superlattices, Adv. Mater. **19**, 4153 (2007).

[3] P. Aguado-Puente, P. Garcia-Fernandez, and J. Junquera, Interplay of Couplings between Antiferrodistortive, Ferroelectric, and Strain Degrees of Freedom in Monodomain $PbTiO_3/SrTiO_3$ Superlattices, Phys. Rev. Lett. **107**, 217601 (2011).

[4] E. Bousquet, M. Dawber, N. Stucki, C. Lichtensteiger, P. Hermet, S. Gariglio, J. M. Triscone, amd P. Ghosez, Improper ferroelectricity in perovskite oxide artificial superlattices, Nature (London) **452**, 732 (2008).

[5] I. Misirlioglu, M. Alexe, L. Pintilie, and D. Hesse, Space charge contribution to the apparent enhancement of polarization in ferroelectric bilayers and multilayers, Appl. Phys. Lett. **91**, 022911 (2007).

[6] V. R. Cooper, K. Johnston, and K. M. Rabe, Polarization enhancement in short period superlattices via interfacial intermixing, Phys. Rev. B **76**, 020103(R) (2007).

[7] S. Das, Y. Tang, Z. Hong, M. Gonçalves, M. McCarter, C. Klewe, K. Nguyen, F. Gómez-Ortiz, P. Shafer, E. Arenholz, V. A. Stoica, S. L. Hsu, B. Wang, C. Ophus, J. F. Liu, C. T. Nelson, S. Saremi, B. Prasad, A. B. Mei, D. G. Schlom, J. Íñiguez, P. García-Fernández *et al.*, Observation of room-temperature polar skyrmions, Nature (London) **568**, 368 (2019).

[8] A. Yadav, C. Nelson, S. Hsu, Z. Hong, J. Clarkson, C. Schlepütz, A. Damodaran, P. Shafer, E. Arenholz, L. Dedon, D. Chen, A. Vishwanath, A. M. Minor, L. Q. Chen, J. F. Scott, L. W. Martin, and R. Ramesh, Observation of polar vortices in oxide superlattices, Nature (London) **530**, 198 (2016).

[9] A. Y. Abid, Y. Sun, X. Hou, C. Tan, X. Zhong, R. Zhu, H. Chen, K. Qu, Y. Li, M. Wu, J. Zhang, J. Wang, K. Liu, X. Bai, D. Yu, X. Ouyang, J. Wang, J. Li, and P. Gao, Creating polar antivortex in $PbTiO_3/SrTiO_3$ superlattice, Nat. Commun. **12**, 2054 (2021).

[10] P. Aguado-Puente and J. Junquera, Structural and energetic properties of domains in $PbTiO_3/SrTiO_3$ superlattices from first principles, Phys. Rev. B **85**, 184105 (2012).

[11] P. Zubko, N. Jecklin, N. Stucki, C. Lichtensteiger, G. Rispens, and J. M. Triscone, Ferroelectric domains in $PbTiO_3/SrTiO_3$ superlattices, Ferroelectrics **433**, 127 (2012).

[12] P. Zubko, J. C. Wojdeł, M. Hadjimichael, S. Fernandez-Pena, A. Sené, I. Luk'yanchuk, J. M. Triscone, and J. Íñiguez, Negative capacitance in multidomain ferroelectric superlattices, Nature (London) **534**, 524 (2016).

[13] S. Das, Z. Hong, M. McCarter, P. Shafer, Y. T. Shao, D. Muller, L. Martin, and R. Ramesh, A new era in ferroelectrics, APL Mater. **8**, 120902 (2020).

[14] B. Kundys, Photostrictive materials, Appl. Phys. Rev. **2**, 011301 (2015).

[15] C. Paillard, X. Bai, I. C. Infante, M. Guennou, G. Geneste, M. Alexe, J. Kreisel, and B. Dkhil, Photovoltaics with ferroelectrics: Current status and beyond, Adv. Mater. **28**, 5153 (2016).

[16] C. Paillard, B. Xu, B. Dkhil, G. Geneste, and L. Bellaiche, Photostriction in Ferroelectrics from Density Functional Theory, Phys. Rev. Lett. **116**, 247401 (2016).

[17] P. Chen, C. Paillard, H. J. Zhao, J. Íñiguez, and L. Bellaiche, Deterministic control of ferroelectric polarization by ultrafast laser pulses, Nat. Commun. **13**, 2566 (2022).

[18] R. Haleoot, C. Paillard, T. P. Kaloni, M. Mehboudi, B. Xu, L. Bellaiche, and S. Barraza-Lopez, Photostrictive Two-Dimensional Materials in the Monochalcogenide Family, Phys. Rev. Lett. **118**, 227401 (2017).

[19] C. Paillard, S. Prosandeev, and L. Bellaiche, *Ab initio* approach to photostriction in classical ferroelectric materials, Phys. Rev. B **96**, 045205 (2017).

[20] B. Peng, Y. Hu, S. Murakami, T. Zhang, and B. Monserrat, Topological phonons in oxide perovskites controlled by light, Sci. Adv. **6**, eabd1618 (2020).

[21] Y. Ahn, J. Park, A. Pateras, M. B. Rich, Q. Zhang, P. Chen, M. H. Yusuf, H. Wen, M. Dawber, and P. G. Evans, Photoinduced Domain Pattern Transformation in Ferroelectric-Dielectric Superlattices, Phys. Rev. Lett. **119**, 057601 (2017).

[22] H. J. Lee, Y. Ahn, S. D. Marks, E. C. Landahl, S. Zhuang, M. H. Yusuf, M. Dawber, J. Y. Lee, T. Y. Kim, S. Unithrattil, S. H. Chun, S. Kim, I. Eom, S. Y. Park, K. S. Kim, S. Lee, J. Y. Jo, J. Hu, and P. G. Evans, Structural Evidence for Ultrafast Polarization Rotation in Ferroelectric/Dielectric Superlattice Nanodomains, Phys. Rev. X **11**, 031031 (2021).

[23] V. Stoica, N. Laanait, C. Dai, Z. Hong, Y. Yuan, Z. Zhang, S. Lei, M. McCarter, A. Yadav, A. Damodaran, S. Das, G. A. Stone, J. Karapetrova, D. A. Walko, X. Zhang, L. W. Martin, R. Ramesh, L. Q. Chen, H. Wen, V. Gopalan *et al.*, Optical creation of a supercrystal with three-dimensional nanoscale periodicity, Nat. Mater. **18**, 377 (2019).

[24] C. Paillard, E. Torun, L. Wirtz, J. Íñiguez, and L. Bellaiche, Photoinduced Phase Transitions in Ferroelectrics, Phys. Rev. Lett. **123**, 087601 (2019).

[25] A. H. Romero, D. C. Allan, B. Amadon, G. Antonius, T. Applencourt, L. Baguet, J. Bieder, F. Bottin, J. Bouchet, E. Bousquet, F. Bruneval, G. Brunin, D. Caliste, M. Coté, J. Denier, C. Dreyer, P. Ghosez, M. Giantomassi, Y. Gillet, O. Gingras, D. R. Hamann *et al.*, ABINIT: Overview and focus on selected capabilities, J. Chem. Phys. **152**, 124102 (2020).

[26] M. Torrent, F. Jollet, F. Bottin, G. Zérah, and X. Gonze, Implementation of the projector augmented-wave method in the ABINIT code: Application to the study of iron under pressure, Comput. Mater. Sci. **42**, 337 (2008).

[27] J. P. Perdew, A. Ruzsinszky, G. I. Csonka, O. A. Vydrov, G. E. Scuseria, L. A. Constantin, X. Zhou, and K. Burke, Restoring the Density-Gradient Expansion for Exchange in Solids and Surfaces, Phys. Rev. Lett. **100**, 136406 (2008).

[28] N. Pertsev, A. Zembilgotov, and A. Tagantsev, Effect of Mechanical Boundary Conditions on Phase Diagrams of Epitaxial Ferroelectric Thin Films, Phys. Rev. Lett. **80**, 1988 (1998).

[29] W. Zhong, R. D. King-Smith, and D. Vanderbilt, Giant LO-TO Splittings in Perovskite Ferroelectrics, Phys. Rev. Lett. **72**, 3618 (1994).

[30] J. B. Neaton and K. M. Rabe, Theory of polarization enhancement in epitaxial $BaTiO_3/SrTiO_3$ superlattices, Appl. Phys. Lett. **82**, 1586 (2003).

[31] Z. Zhu, B. Wang, H. Wang, Y. Zheng, and Q. Li, First-principle study of ferroelectricity in $PbTiO_3/SrTiO_3$ superlattices, Solid-State Electron. **50**, 1756 (2006).

[32] J. Junquera, M. H. Cohen, and K. M. Rabe, Nanoscale smoothing and the analysis of interfacial charge and dipolar densities, J. Phys.: Condens. Matter **19**, 213203 (2007).

[33] A. Baldereschi, S. Baroni, and R. Resta, Band Offsets in Lattice-Matched Heterojunctions: A Model and First-Principles Calculations for GaAs/AlAs, Phys. Rev. Lett. **61**, 734 (1988)

[34] See Supplemental Material at http://link.aps.org/supplemental/10.1103/PhysRevB.106.L220101 for details on the macroaveraging procedure as implemented in ABINIT (Sec. 1) and for another electrostatic model (Sec. 2).

[35] Q. Kong, T. Siauw, and A. Bayen, *Python Programming and Numerical Methods: A Guide for Engineers and Scientists* (Academic Press, Cambridge, MA, 2020).

[36] M. Sepliarsky, S. R. Phillpot, D. Wolf, M. G. Stachiotti, and R. L. Migoni, Long-ranged ferroelectric interactions in perovskite superlattices, Phys. Rev. B **64**, 060101(R) (2001).

[37] K. G. Lim, K. H. Chew, L. H. Ong, and M. Iwata, Electrostatic coupling and interface intermixing in ferroelectric superlattices, Europhys. Lett. **99**, 46004 (2012).

[38] A. L. Roytburd, S. Zhong, and S. P. Alpay, Dielectric anomaly due to electrostatic coupling in ferroelectric-paraelectric bilayers and multilayers, Appl. Phys. Lett. **87**, 092902 (2005).

[39] P. Delugas, A. Filippetti, and V. Fiorentini, Spontaneous 2-Dimensional Carrier Confinement at the *n*-Type $SrTiO_3/LaAlO_3$ interface, Phys. Rev. Lett. **106**, 166807 (2011).

[40] M. Stengel, First-Principles Modeling of Electrostatically Doped Perovskite Systems, Phys. Rev. Lett. **106**, 136803 (2011).

[41] F. Berz, A simplified theory of the p-i-n diode, Solid-State Electron. **20**, 709 (1977).

[42] B. G. Streetman and S. Banerjee, *Solid State Electronic Devices* (Pearson/Prentice Hall, Upper Saddle River, NJ, 2006).

[43] B. J. Baliga, *Fundamentals of Power Semiconductor Devices* (Springer, New York, 2010).

[44] P. Aguado-Puente, N. C. Bristowe, B. Yin, R. Shirasawa, P. Ghosez, P. B. Littlewood, and E. Artacho, Model of two-dimensional electron gas formation at ferroelectric interfaces, Phys. Rev. B **92**, 035438 (2015).

[45] B. Yin, P. Aguado-Puente, S. Qu, and E. Artacho, Two-dimensional electron gas at the $PbTiO_3/SrTiO_3$ interface: An *ab initio* study, Phys. Rev. B **92**, 115406 (2015).

[46] E. A. Eliseev, S. V. Kalinin, and A. N. Morozovska, Finite size effects in ferroelectric-semiconductor thin films under open-circuit electric boundary conditions, J. Appl. Phys. **117**, 034102 (2015).

[47] L. Bellaiche, A. García, and D. Vanderbilt, Finite-Temperature Properties of $PbZr_{(1-x)}Ti_xO_3$ Alloys from First Principles, Phys. Rev. Lett. **84**, 5427 (2000).

[48] L. Bellaiche, A. García, and D. Vanderbilt, Low-temperature properties of $PbZr_{(1-x)}Ti_xO_3$ solid solutions near the morphotropic phase boundary, Ferroelectrics **266**, 41 (2002).

[49] L. Chen, Y. Yang, Z. Gui, D. Sando, M. Bibes, X. K. Meng, and L. Bellaiche, Large Elasto-Optic Effect in Epitaxial $PbTiO_3$ Films, Phys. Rev. Lett. **115**, 267602 (2015).

[50] C. Paillard, S. Prokhorenko, and L. Bellaiche, Strain engineering of electro-optic constants in ferroelectric materials, npj Comput. Mater. **5**, 1 (2019).